J Mater Sci: Mater Med (2009) 20:S43–S48
DOI 10.1007/s10856-008-3480-8

Hydrothermal synthesis of porous triphasic hydroxyapatite/(α and β) tricalcium phosphate

R. Vani · E. K. Girija · K. Elayaraja · S. Prakash Parthiban · R. Kesavamoorthy · S. Narayana Kalkura

Received: 31 October 2007 / Accepted: 19 May 2008 / Published online: 17 June 2008

Abstract A novel, porous triphasic calcium phosphate composed of nonresorbable hydroxyapatite (HAp) and resorbable tricalcium phosphate (α- and β-TCP) has been synthesized hydrothermally at a relatively low temperature. The calcium phosphate precursor for hydrothermal treatment was prepared by gel method in the presence of ascorbic acid. XRD, FT-IR, Raman analyses confirmed the presence of HAp/TCP. The surface area and average pore size of the samples were found to be 28 m^2/g and 20 nm, respectively. The samples were found to be bioactive in simulated body fluid (SBF).

1 Introduction

Hydroxyapatite [$Ca_{10}(PO_4)_6(OH)_2$] is one of the most important biomaterial widely used in biomedical field due to its biocompatibility, bioactivity and osteoconductivity. It has been widely used for hard tissue replacement materials such as bone and teeth [1–3]. HAp is also used in non-load bearing applications, such as the ossicles of the middle ear, orthopedic bone grafting due to its poor mechanical properties [4]. On the other hand HAp coated implants are used in load bearing applications to promote bone formation [5]. Porous HAp improves the mechanical interlock between the cells and the surface of the material and promotes osteoconductivity [6]. The rate of integration and the volume of newly regenerated bone have been shown to be dependent on porosity, pore size and the path of pore connectivity [7]. However, owing to the nonresorbable nature of HAp, current research is focused on the mixture of calcium phosphates, which contains most stable phase of HAp and soluble phase of tricalcium phosphate (TCP) [8–10]. HAp/TCP has enhanced osteoconductivity and osteogenesis which accelerates the bone formation [11]. Dissolution of TCP in HAp/TCP releases calcium and phosphate ions into biological medium and act as a seed for new bone formation [12, 13]. HAp/TCP is also widely used in drug adsorption and release [14]. Different routes are used to prepare the mixture of HAp/TCP viz, solid state reaction, precipitation, combustion, hydrothermal, microwave processing and sintering of calcium deficient hydroxyapatite at or above 700°C [15–20]. In most of the methods HAp/TCP is obtained after sintering. Due to sintering, the functional groups of HAp/TCP may lose its bioactivity and also could lead to closer of interconnection between the pores which could affect the transportation of body fluid and nutrition during bone regeneration, and delay the bone formation. On the other hand, TCP have been prepared as a biomaterial and replaced by new bone growth as they degrade due to its resorbability [21]. It is a challenge to synthesize the highly biodegradable α- and β-TCP at low temperature because α-TCP is a high temperature phase and crystallized at the temperature 1,120°C [22] and β-TCP is not a stable phase at room temperature. Li et al. highlighted the importance and advantages of

R. Kesavamoorthy is deceased.

R. Vani · K. Elayaraja · S. Prakash Parthiban · S. Narayana Kalkura (✉)
Crystal Growth Centre, Anna University, Chennai 600 025, India
e-mail: kalkura@annauniv.edu; kalkura@yahoo.com

E. K. Girija
School of Physics, Madurai Kamaraj University, Madurai 625 021, India

R. Kesavamoorthy
Materials Science Division, IGCAR, Kalpakkam 603 102, India

biodegradation of the mixture of α- and β-TCP and they synthesized α- and β-TCP at 800°C [23]. Here we report, a novel low temperature hydrothermal method to prepare the highly biodegradable porous HAp/TCP (α and β). Precursor was prepared in the presence of ascorbic acid in gel method under physiological condition. Ascorbic acid (AA) plays an essential role in synthesis of collagen [24, 25].

2 Materials and method

All the reagents used for this experiment were of an analar grade procured from Merck, India and were used without any further purification.

Calcium phosphate precursor was prepared by gel method in single diffusion technique and then subjected to hydrothermal treatment. The experimental procedure was as shown in the flow chart given below.

The gel was prepared by mixing SMS-sodium meta silicate (Qualigens) solution of specific gravity 1.03 g/cm^3 and 0.6 M of di sodium hydrogen phosphate (Na_2HPO_4) in the ratio 1:1. To this, 50 mM of ascorbic acid was added after that the pH of the solution was adjusted to 7.4 using 10% acetic acid. The same solution without AA was used as blank. The solution was allowed to gel. After the gelation, 1 M $CaCl_2 \cdot 2H_2O$ was used as the supernatant solution. The experiments were carried out at 37°C (±0.1°C).

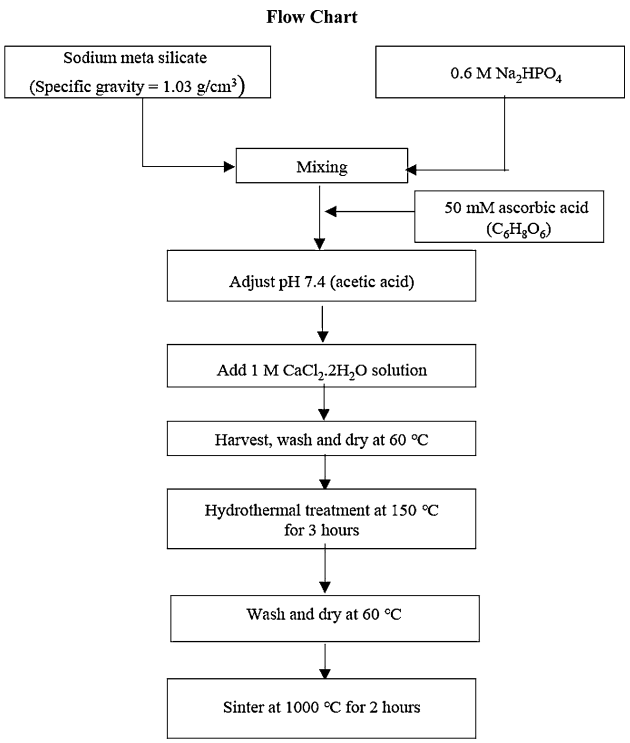

After the crystallization was complete, the samples were harvested, washed with double distilled water and dried at 60°C. This sample was used as a precursor for hydrothermal treatment at 150°C for 3 h. After hydrothermal treatment the sample was washed with double distilled water and dried at 60°C. The product was sintered at 1,000°C for 2 h.

The samples were characterized by X-ray powder diffraction (XRD) using RINT 2200, Rigaku diffractometer. Ni-filtered Cu-K_α radiation ($\lambda = 1.5405$ Å) operated at 40 kV/30 mA at the 2θ range of 20–60° in continuous scan mode at a scanning speed of 0.02°. The Fourier transform infrared spectrum (FT-IR) was recorded in PERKIN ELMER Spectrum RX1 using KBr pellet technique for the range 4,000 and 400 cm^{-1}. Raman spectrum of the sample was recorded at room temperature in the back scattering geometry using a Laser—Raman spectrometer built around a double grating monochromator (SPEX, model 14018). The sample was excited with 488 nm argon ion laser beam of 40 mW focused to a spot size of 100 μm on the sample. N_2 adsorption–desorption measurements were carried out on a Micromeritics ASAP 2020 gas adsorption analyzer, after out gassing the samples at 200°C overnight on a vacuum line. The surface areas were calculated by the BET method and the pore size distributions were calculated from the desorption branch of the isotherm.

3 Results and discussion

The addition of $CaCl_2 \cdot 2H_2O$ as the supernatant solution, led to the formation of a white precipitate at the gel–solution interface. Within a day, periodic disc of white precipitate (Liesegang Rings-LRs) were observed just below the interface precipitate and continued to develop over a period of time. In the presence of ascorbic acid more number of LRs were observed. This indicates that AA accelerates the formation of calcium phosphate. The harvested LRs grown in the presence of AA were subjected to hydrothermal treatment. LRs were not in direct contact with water. The LRs reacted with water vapor leading to their recrystallization under hydrothermal conditions.

Calcium phosphate prepared by gel method and hydrothermally treated samples were identified as the mixture of HAp and α- and β-TCP from XRD (Fig. 1a, b) which is in good agreement with the JCPDS standards (09-0432, 09-0348 and 09-0169). The hydrothermally treated sample (Fig. 1b) showed sharp and distinct peaks for the planes (211), (112), (300) which indicate better crystallinity compared to the as prepared sample. The characteristic peak of β-TCP appeared in both as prepared and hydrothermally treated, as a weak shoulder peak (Fig. 1 insert). There were no new crystalline phase other than HAp and

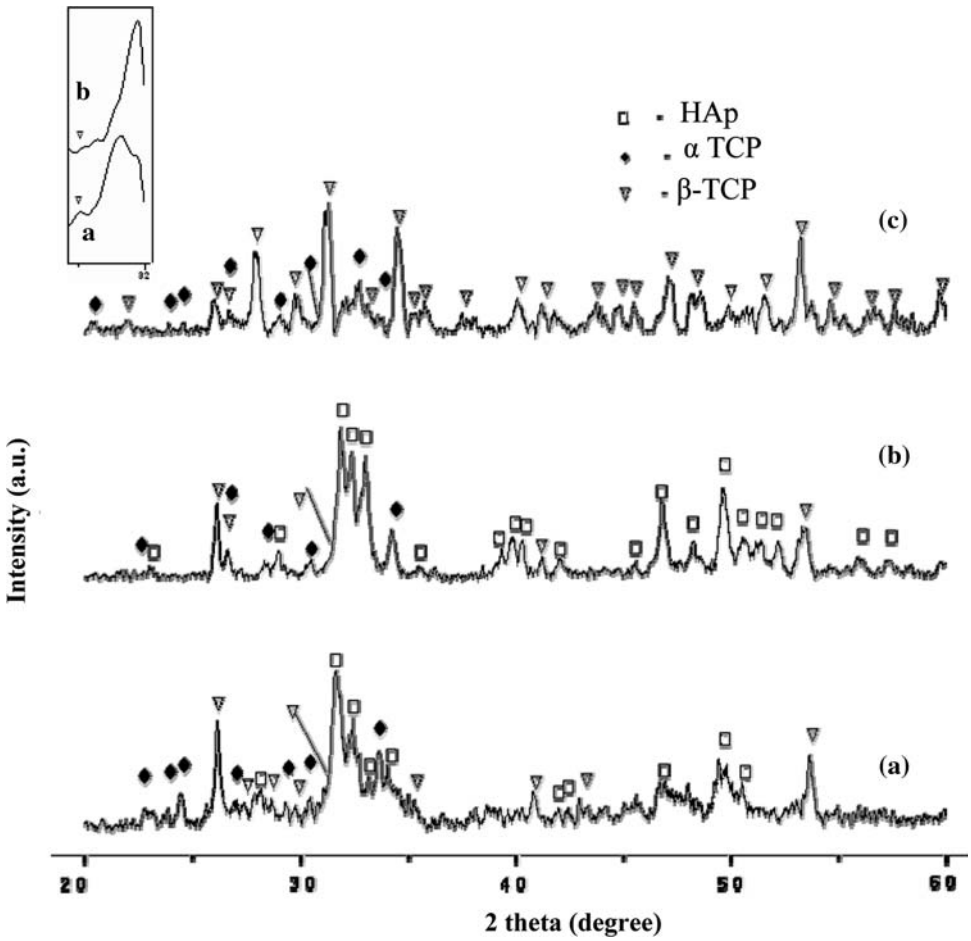

Fig. 1 XRD patterns of (a) as prepared (b) hydrothermally treated and (c) sintered at 1,000°C. Insert—magnified pattern of XRD from 29.7° to 32° showed a characteristic shoulder peak corresponding to β-TCP

TCP. The crystallinity of HAp/TCP was 85%, as deduced from the integrated intensity (Area) of the amorphous peak (310) and the crystalline peak (211) of HAp using the relation $I_C/(I_C + I_A)$ [26]. The peaks corresponding to α-TCP appeared in both as prepared and hydrothermally treated samples, confirms the formation of α-TCP even at physiological temperature. The XRD patterns of sintered sample indicated the presence of α- and β-TCP (Fig. 1c). There was a complete decomposition of HAp into α- and β-TCP at 1,000°C.

Figure 2 illustrates the FT-IR absorption spectra of the hydrothermally treated sample. The band at 1,030 cm^{-1} is assigned to the triply degenerate v_3 asymmetric P–O stretching mode. The peak at 961 cm^{-1} is attributed to v_1, the non-degenerate P–O symmetric stretching mode. The bands at 601 and 562 cm^{-1} correspond to the triply degenerate v_4, O–P–O bending mode and the band at 476 cm^{-1} is attributed to the doubly degenerate v_2, O–P–O bending mode. Low intensity OH^- derived band is observed at 630 cm^{-1}. The bands at 1,641 and 3,417 cm^{-1} are assigned to the adsorbed water. In addition, the weak peak at 866 cm^{-1} is due to the P–O(H) stretch of HPO_4^{2-}, indicate the presence of calcium deficient HAp [27].

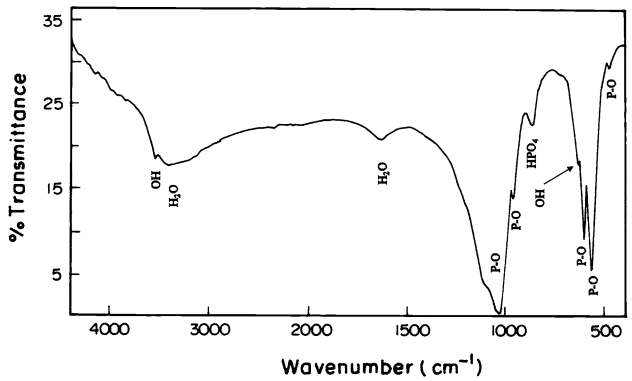

Fig. 2 FT-IR spectra of the hydrothermally treated HAp/TCP

The weak band at 3,558 cm^{-1} is attributed to OH bending mode. The low intensity hydroxyl group at 630 and 3,558 cm^{-1} indicate the presence of HAp/TCP [19].

The Raman spectrum of hydrothermally treated sample is as shown in Fig. 3. The band at 960 cm^{-1} is assigned to the strongest v_1, P–O stretching mode of HAp. The Shoulder peak observed at 988 cm^{-1} is assigned to P–O stretching and indicated the presence of α-TCP [28]. The

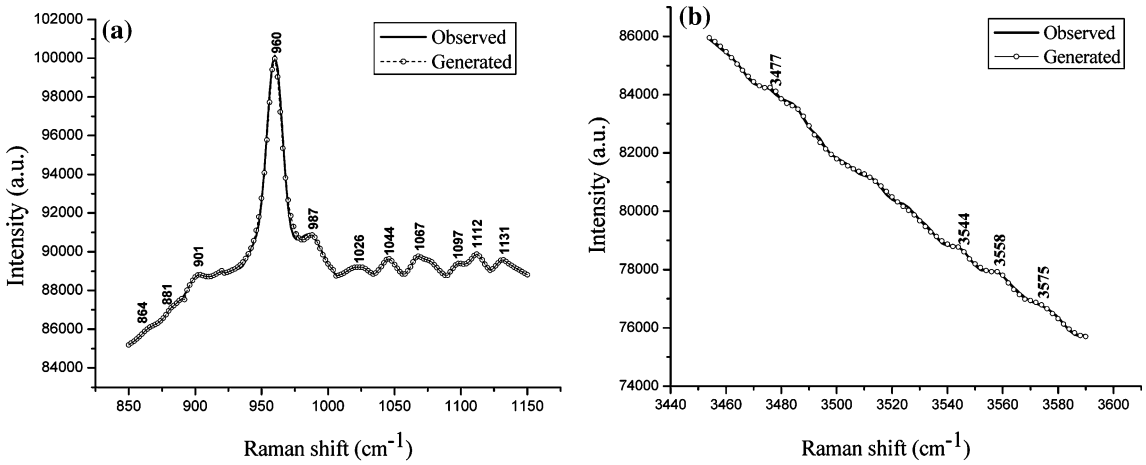

Fig. 3 Raman spectrum of the hydrothermally treated HAp/TCP (**a**) PO_4^{3-} mode and (**b**) OH^- mode

bands observed in the region 1,000–1,150 cm^{-1} are attributed to v_3, P–O stretching mode. The splitting of peaks at 864 and 881 cm^{-1} corresponds to HPO_4^{2-} [29]. The bands at 426, 527 and 554 cm^{-1} are assigned to v_2, O–P–O doubly degenerated bending mode. The peaks at 588 and 615 cm^{-1} are attributed to v_4, O–P–O triply degenerated bending mode. The splitting of peaks at v_3 (1026, 1044, 1067, 1097 and 1112 cm^{-1}) are suggested the co-existence of HAp, α- and β-TCP [28]. The low intensity bands at 3,558 cm^{-1} and 3,575 cm^{-1} are assigned to bending mode of O–H group (Fig. 3b). The Raman assignments of the characteristic bands are given in Table 1.

SEM micrograph of the as prepared sample in the presence of AA (Fig. 4b) showed the spherulites of diameter 5–15 μm whereas the sample prepared without AA contain acicular crystals of length 5–10 μm (Fig. 4a). Here AA seems to inhibit the growth along the c-axis leading to the formation of spherulites. Hydrothermally treated sample revealed the interconnected porous network of pore size around 5 μm along with hexagonal and rectangular crystals with edges of around 10–50 μm (Fig. 4c, d).

The nitrogen adsorption–desorption isotherm (Fig. 5) of hydrothermally treated sample exhibit type IV hysteresis loop, indicated the presence of ink-bottle type mesopores [30]. The Brunauer–Emmett–Teller (BET) surface area of the sample was measured to be 28 m^2/g. The sample has mesopores of average pore size 20 nm.

To check the bioactivity, the hydrothermally treated sample was immersed in 10 ml of simulated body fluid (SBF) with an ionic concentration nearly equal to that of human blood plasma kept at 37 ± 0.1°C for a week. SBF was prepared by dissolving NaCl, $NaHCO_3$, KCl, $K_2HPO_4 \cdot 3H_2O$, $MgCl_2 \cdot 6H_2O$, 1 M HCl, $CaCl_2 \cdot 2H_2O$, Na_2SO_4 and $(CH_2OH)_3\ CNH_2$ in de-ionized water and buffered to pH 7.4 at 37 ± 0.1°C with HCl [31]. Before soaking into SBF the sample was weighed (W_1). When the sample was immersed in SBF there was a slight reduction in pH, subsequently after 2 days there was an increase in pH due to the ion exchange between the sample and SBF. After a week the sample was taken out and washed with de-inoized water and dried at 60°C and weighed (W_2). The sample was subsequently observed under SEM which revealed the apatite deposition on the surface of the sample

Table 1 Raman assignments (Lorentzian) of hydrothermally treated HAp/TCP

Vibrational Raman mode			Assignments
Peak center (cm^{-1})	FWHM (cm^{-1})	Area (a.u)	
426	16.85	31839	O–P–O doubly degenerated bending
527	22.76	12839	
554	29.07	21596	
588	22.96	58064	O–P–O triply degenerated bending
615	15.86	7486	
864	14.42	4863	HPO_4^{2-} mode
881	12.68	6639	
960	15.12	247027	P–O stretching (triply degenerated)
988	17.51	41429	P–O stretching mode
1026	11.75	4310	P–O asymmetric stretching mode
1044	15.66	18346	
1067	12.81	14997	
1097	14.56	12317	
1112	14.84	20886	
3477	14.24	15683	O–H stretching of water
3544	04.10	3190	O–H stretching
3558	06.92	3629	
3575	25.31	19370	

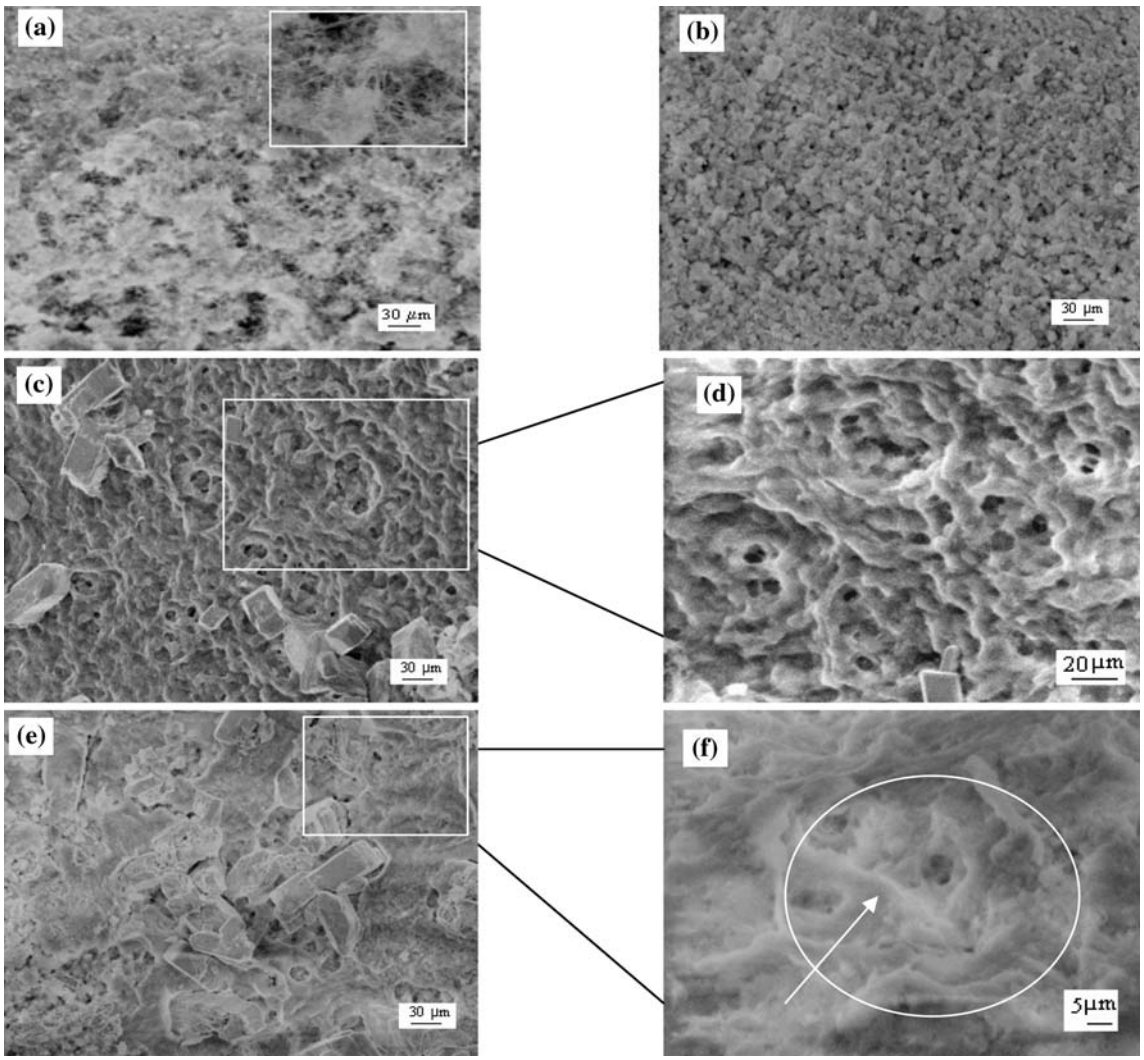

Fig. 4 SEM morphology for (**a**) In the absence of ascorbic acid—acicular crystals of length 5–10 µm. (**b**) Precursor prepared in the presence of ascorbic acid—spherulites of 5–15 µm diameter. (**c** and **d**) Hydrothermally treated HAp/TCP prepared in the presence of ascorbic acid—Porous network with hexagonal and rectangular crystals of edge10–50 µm. (**e**) Apatite layer formation on HAp/TCP in SBF. (**f**) Magnified portion of figure (**e**)—arrow indicate the deposition of apatite layer on porous network

(Fig. 4e, f). The difference in weight before and after soaking of SBF ($W_2 - W_1$) showed an increase in weight further confirming the deposition of apatite layer on to the surface of the sample. The partial dissolution of TCP increases the local supersaturation of calcium and phosphate ions in SBF, leading to the deposition of the apatite layer on the sample [32].

4 Conclusions

This study presents, a novel hydrothermal method to prepare a porous network of HAp/(α and β)TCP at low temperature than the other existing methods reported in literature. Ascorbic acid is found to accelerate the calcium phosphate agglomeration under physiological conditions. The presence of the mixture of HAp/TCP in hydrothermally treated sample was confirmed by XRD, FT-IR and Raman analyses. Specific surface area and average pore size of HAp/TCP was 28 m^2/g and 20 nm (mesopores), respectively. The porous nature of the samples enables the circulation of body fluids and nutrition which enhances its biocompatibility. Further the mesopores may help in effective drug adsorption and release. In vitro study showed excellent bioactivity of hydrothermally treated sample in SBF. Hence this process could emerge as a novel route to produce HAp/TCP at low temperature for biomedical applications due to its biodegradability.

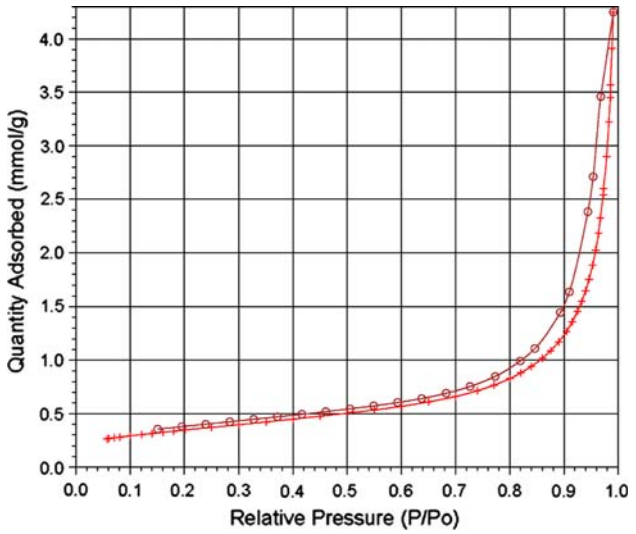

Fig. 5 Nitrogen adsorption–desorption isotherm of hydrothermally treated HAp/TCP

Acknowledgements The authors acknowledge the grant from Department of Science and Technology, New Delhi through Research Project No. SR/SO/HS-05/2005. The authors wish to thank Dr. M. Palanichamy, Department of Chemistry, Anna University, Chennai for useful discussions.

References

1. M. Vallet-Regi, J.M. Gonzalez-Calbet, Prog. Solid State Chem. **32**, 1–31 (2004)
2. P.N. Kumta, C. Sfeir, D.-H. Lee, D. Olton, D. Choi, Acta Biomater. **1**, 65–83 (2005)
3. W. Suchanek, M. Yoshimura, J. Mater. Res. **13**, 94–115 (1998)
4. G. Goller, F.N. Oktar, S. Agathopoulos, D.U. Tulyaganov, J.M.F. Ferreira, E.S. Kayali, Z. Peker, J. Sol-Gel Sci. Techn. **37**, 111–115 (2006)
5. I.-H. Oh, N. Nomura, A. Chiba, Y. Murayama, N. Masahasht, B.-T. Lee, S. Hanada, J. Mater. Sci.: Mater. Med. **16**, 635–640 (2005)
6. D. Tadic, F. Beckmann, K. Schwarz, M. Epple, Biomaterials **25**, 3335–3340 (2004)
7. I. Manjubala, A. Woesz, C. Pilz, M. Rumpler, N. Fratzl-Zelman, P. Roschger, J. Stampfl, P. Fratzl, J. Mater. Sci.: Mater. Med. **16**, 1111–1119 (2005)
8. T.L. Arinzeh, T. Tran, J. Mcalary, G. Daculsi, Biomaterials **26**, 3631–3638 (2005)
9. P. Looss, A.-M. Le Ray, G. Frimandi, G. Daculsi, C. Merle, Biomaterials **22**, 2785–2794 (2001)
10. C.R. Yang, Y.J. Wang, X.F. Chen, N.R. Zhao, Mater. Lett. **59**, 3635–3640 (2005)
11. Y. Xie, D. Chopin, C. Morin, P. Hardouin, Z. Zhu, J. Tang, J. Lu, Biomateirals **27**, 2761–2767 (2006)
12. G. Daculsi, Biomaterials **19**, 1473–1478 (1998)
13. G. Daculsi, R.Z. Legeros, E. Nery, K. Lynch, B. Kerebel, J. Biomed. Mat. Res. **23**, 883–894 (1989)
14. M. Sunder, N. Ramesh Babu, P. Sunita, K. Ram Kumar, T.S. Sampath Kumar, Trends Biomater. Artif. Organs. **18**, 213–218 (2005)
15. X. Yang, Z. Wang, J. Mater. Chem. **8**, 2233–2237 (1998)
16. N. Kivrak, A.C. Tas, J. Am. Ceram. Soc. **81**, 2245–2252 (1998)
17. A.C. Tas, J. Euro. Ceram. Soc. **20**, 2389–2394 (2000)
18. K. Ozeki, H. Aoki, Y. Fukui, J. Mater. Sci. **40**, 2837–2842 (2005)
19. I. Manjubala, M. Sivakumar, Mater. Chem. Phys. **71**, 272–278 (2001)
20. M. Tamai, T. Isshiki, K. Nishio, M. Nakamura, A. Nakahira, H. Endoh, J. Mater. Sci. **41**, 525–530 (2006)
21. D. Choi, P.N. Kumta, Mater. Sci. Eng. **C27**, 377–381 (2007)
22. S.V. Dorozhkin, M. Epple, Angew Chem Int Ed **41**, 3130–3146 (2002)
23. Y. Li, W. Weng, K.C. Tam, Acta Biomater. **3**, 251–254 (2007)
24. J.J. Jeffrey, G.R. Martin, Biochim. Biophys. Acta (BBA) **121**, 281–291 (1966)
25. M. Ogawara, K. Aoki, T. Okiji, H. Suda, Arch. Oral Biol. **42**, 695–704 (1997)
26. A. Benlhachemi, S. Golec, J.R. Gavarri, Physica C **209**, 353 (1993)
27. M.A. Verges, C.F. Gonzalez, M.M. Gallego, J. Euro. Ceram. Soc. **18**, 1245–1250 (1998)
28. H. Li, B.S. Ng, K.A. Khor, P. Cheang, T.W. Clyne, Acta Mater. **52**, 445–453 (2004)
29. R.M. Wilson, J.C. Elliott, S.E.P. Dowker, L.M. Rodriguez-Lorenzo, Biomaterials **26**, 1317–1327 (2005)
30. S.B. Cho, F. Miyaji, T. Kokubo, K. Nakanishi, N. Soga, T. Nakamura, J. Mater. Sci.: Mater. Med. **9**, 279–284 (1998)
31. T. Kokubo, H. Takadama, Biomaterials **27**, 2907–2915 (2006)
32. C. Ribeiro, E.C.S. Rigo, P. Sepulveda, J.C. Bressiani, A.H.A. Bressiani, Mater. Sci. Eng. **C24**, 631–636 (2004)